Ab Initio Study of the Thiolysis of Trimethyl Phosphate Ester in the Gas Phase

Guilherme Menegon,* Michel Loos, and Hernan Chaimovich

Instituto de Química, Universidade de São Paulo, Av. Lineu Prestes 748, 05508-900, São Paulo, SP, Brazil

Received: May 7, 2002; In Final Form: August 5, 2002

Phosphate esters are key compounds in important biological reactions. One family of enzymes, PTPases, catalyze the dephosphorylation of tyrosine residues from other proteins by a cystein side-chain nucleophilic attack at tyrosin phosphate. Very little is known about the intrinsic reactivity of thiol nucleophiles with phosphorus centers. To explore this important reaction, we have performed ab initio calculations on the trimethyl phosphate ester (TMP) thiolysis by $(CH_3S)^-$. Results in the gas phase indicate that attack at TMP carbon is essentially predominant over phosphorus. Mechanisms are A_nD_n and exoergic for reaction at carbon and $A_n + D_n$ with large activation barriers and endoergic reaction for attack on phosphorus. A trigonal-bipyramid intermediate was formed upon $(CH_3S)^-$ reaction at phosphorus and two different and competitive pathways were found for the elimination of methoxide from this intermediate. One of the elimination pathways is positioned in-line to the thiol group, as proposed in the enzymatic mechanism. If PTPases work by the same mechanism as the gas-phase reaction, these enzymes should drastically lower the activation barriers for attack at phosphorus.

1. Introduction

Phosphate esters control a significant part of living world chemistry.[1] From genetic material and coenzymes to energy-storing compounds and signalling agents, phosphate esters are ubiquitous. Pesticides and chemical warfare nerve agents are also derived from phosphate esters. Nucleophilic reactions of phosphate esters, mostly hydrolysis and alcoholysis, have been studied in solution,[2−5] gas phase,[6−8] and computationally.[9−11] Phosphate ester thiolysis, a biologically important reaction, however, has received less attention and to our knowledge the only report of thiol nucleophilic attack at phosphorus is the intramolecular reactivity of a thio nucleotide analog.[12]

The phosphate ester thiolysis is an important biochemical reaction because a large family of phosphatases (see the recent *Chemical Reviews* special issue[13]) catalyze the dephosphorylation of proteins and peptides through the formation of a thiophosphate intermediate.[14,15] The active site of protein tyrosin phosphatases (PTPases) has a reactive cystein whose side-chain[14,16] attacks the phosphorus atom of phosphorylated tyrosin residues[14] from other proteins yielding a phosphorylated PTPase intermediate which is then hydrolyzed.[15,17]

Numerous questions on the reactivity of phosphate esters are still open. The age-old question is whether the nucleophilic attack toward phosphate esters proceeds through an associative or dissociative mechanism.[9,18,19] This seems to be controlled by the alkylation and charge state of the phosphate ester[18] but one would like to probe the influence of the thiolate nucleophile. Another open question is whether trigonal-bipyramidal (TBP) intermediates are always formed in a nucleophilic reaction at the phosphorus center.[20,21]

Ab initio calculations on the phosphate ester thiolysis in the gas phase may help to understand the intrinsic features of this reaction. We have chosen a simple model system to employ correlated electronic structure methods with a suitable calculation cost. The nucleophile is thiomethoxide, $(CH_3S)^-$, and the ester is trimethyl phosphate, TMP. We have chosen a triester because a neutral mono or diester would involve intramolecular proton transfer which would obscure the intrinsic reactivity. Although a mono- or dianion phosphate would be a more realistic representation of the PTPase enzymatic substrate,[14] we are unsure about running accurate gas-phase calculations with a limited basis set in tri- or double-negative charged species.

SCHEME 1: $(CH_3S)^-$ Attack at TMP Carbon and Phosphorus

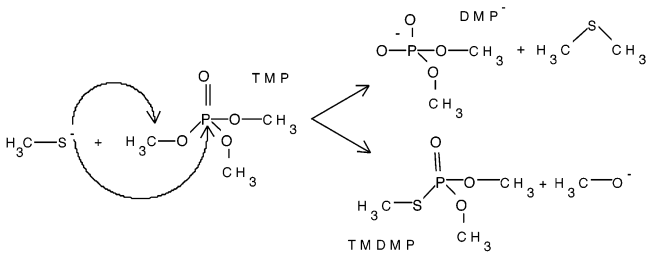

As noted below, we have calculated free energies which do not contain thermal contributions because vibrational entropy (S_{vib}) can be a significant source of error in thermochemical calculations.[22] One can compare, for example, the calculations of the same phosphate esters alcoholysis and hydrolysis by Warshel et al. who employed the MP2/6-31+G**//HF/6-31G* level of theory (see reactions 13 and 17 of their paper)[9] and by Pedersen et al. at the MP2/6-31+G* level (see reactions 4 and 3 of their paper, respectively).[23] Although the differences in reaction energy between these two studies, including only electronic and nuclear repulsion contributions, are only 0.2 and 0.3 kcal/mol, the differences in reaction entropy, calculated with the same methodology,[24] are 4.8 and 4.6 kcal/mol at 298 K, respectively. These differences result in considerable disagreement between the calculated free energies.[9,23]

With TMP as a substrate, nucleophiles can attack at carbon and phosphorus and both pathways were analysed here (Scheme 1). The experimental gas-phase studies of Lum and Grabowski[7]

* Corresponding author. E-mail: garantes@iq.usp.br.

10.1021/jp026083i CCC: $22.00
Published on Web 08/30/2002

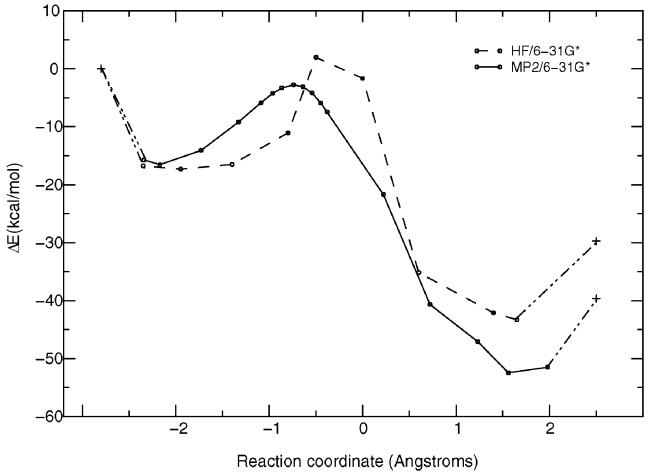

Figure 1. Relative MP2/6-31G* and HF/6-31G* energies for the gas-phase reaction of $(CH_3S)^-$ at the TMP carbon. Indicated by a plus(+) symbol, reactants and products at large separation (30 Å) are out of the reaction coordinate scale.

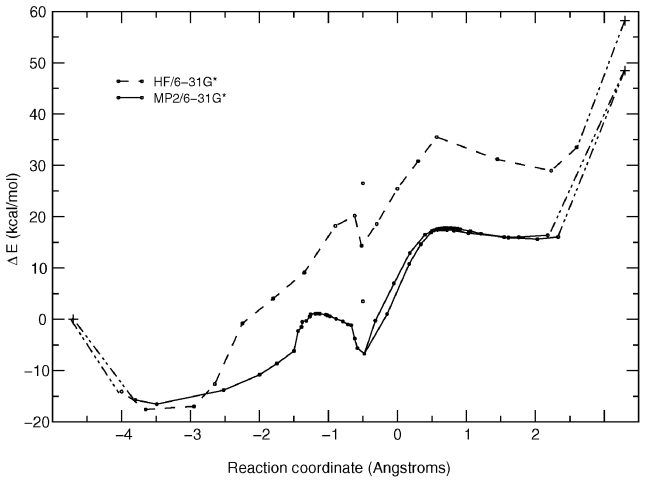

Figure 2. Relative MP2/6-31G* and HF/6-31G* energies for the gas-phase reaction of $(CH_3S)^-$ at the TMP phosphorus. Indicated by a plus-(+) symbol, reactants and products at large separation (30 Å) are out of the reaction coordinate scale.

with a series of nucleophiles (including hydrogen sulfide, $(HS)^-$) and the calculations by Lim et al. of hydroxide, methoxide, and fluoride reactions with TMP were used for comparisons.

Details of the calculations are described in the Methods section. Reaction coordinates, free energy profiles, and mechanisms are described in the Results section. In the Discussion section, we further develop our analysis on the TMP thiolysis and compare our findings with those of other similar studies.

2. Methods

Calculations were carried out with the Gaussian 98 program system.[25] Partial potential energy surfaces and reaction pathways were evaluated in the gas phase using the 6-31G* basis set. All stationary geometries, reactants, and products were fully re-optimized using the 6-311++G* basis set. The restricted Hartree-Fock (HF) level and the second-order Møller-Plesset (MP2) perturbation theory[26] at the frozen core approximation were used. Geometries were optimized in both levels by the analytic gradient method. Stationary points (minima and transition states) were fully optimized and the other geometries were partially optimized by freezing the forming (breaking) bond distance. Geometries near TS1 (Figure 4) had both forming and breaking bond distances frozen and geometries near TS2 had two dihedral angles (C1−S−P−O1 and C2−O2−P−O1, Figure 4) constrained. Each species were separated by 30 Å in the bimolecular reactants and products calculations. Analytical vibrational frequencies were calculated at the HF and MP2 levels of theory for the respective stationary points. No imaginary frequencies were found for minima and only one imaginary frequency was found for the transition states (TS). Intrinsic reaction coordinate (IRC)[27] were followed[28] from all TS and led in the direction of the expected reactants and products.

During vibrational analysis in all geometries, the lowest 6 real roots of the mass-weighted Hessian eigenvalues were checked and found to be smaller than 3 cm^{-1}.[29] Vibrational frequencies calculated at the MP2 level were also used to obtain the zero-point energy (E_{ZPE}). No empirical scaling was applied to frequencies (vibrational frequencies for TMP calculated at the MP2/6-31G* level[30] are overestimated by 1.2% to at most 4.0% in comparison to experimental ones). Addition of the zero-point energy (E_{ZPE}) obtained from frequency calculations at the MP2/6-31G* level to the electronic and nuclear repulsion energy

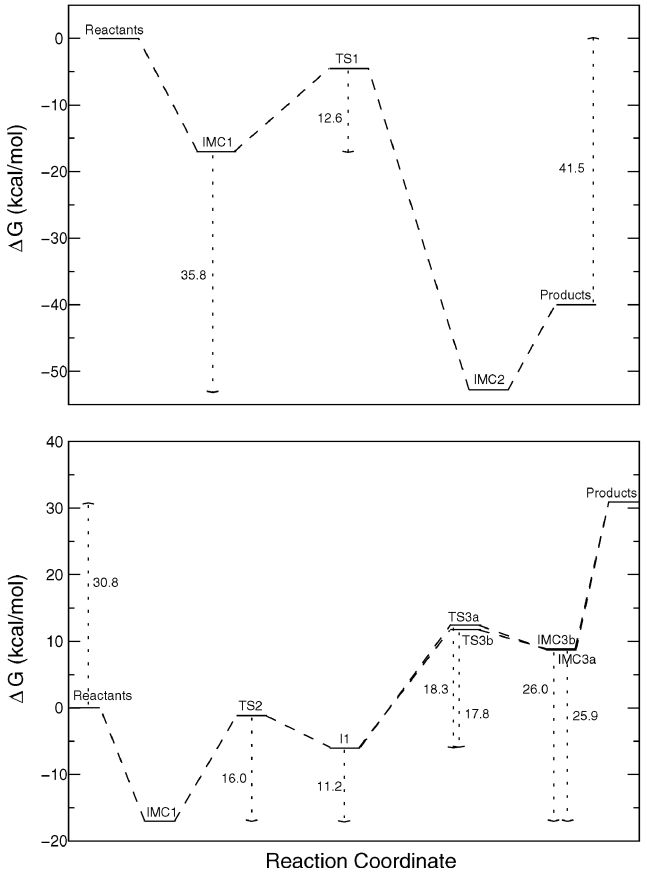

Figure 3. Relative free energy profiles at 0 K for the gas-phase reaction of $(CH_3S)^-$ at the TMP carbon (top) and phosphorus (bottom), $\Delta G = \Delta E_{MP2} + \Delta E_{ZPE}$.

(E_{MP2}) obtained at the MP2/6-311++G* level resulted in the gas-phase free energy at 0 K, $G = E_{MP2} + E_{ZPE}$.

3. Results

Reaction pathways (Figures 1and 2) and comparisons between HF and MP2 levels are based on the calculations with the 6-31G* basis set. Free energy profiles (Figure 3) and structures optimized at the MP2 level representative of stationary points (Figure 4) were obtained from calculations with the 6-311++G*

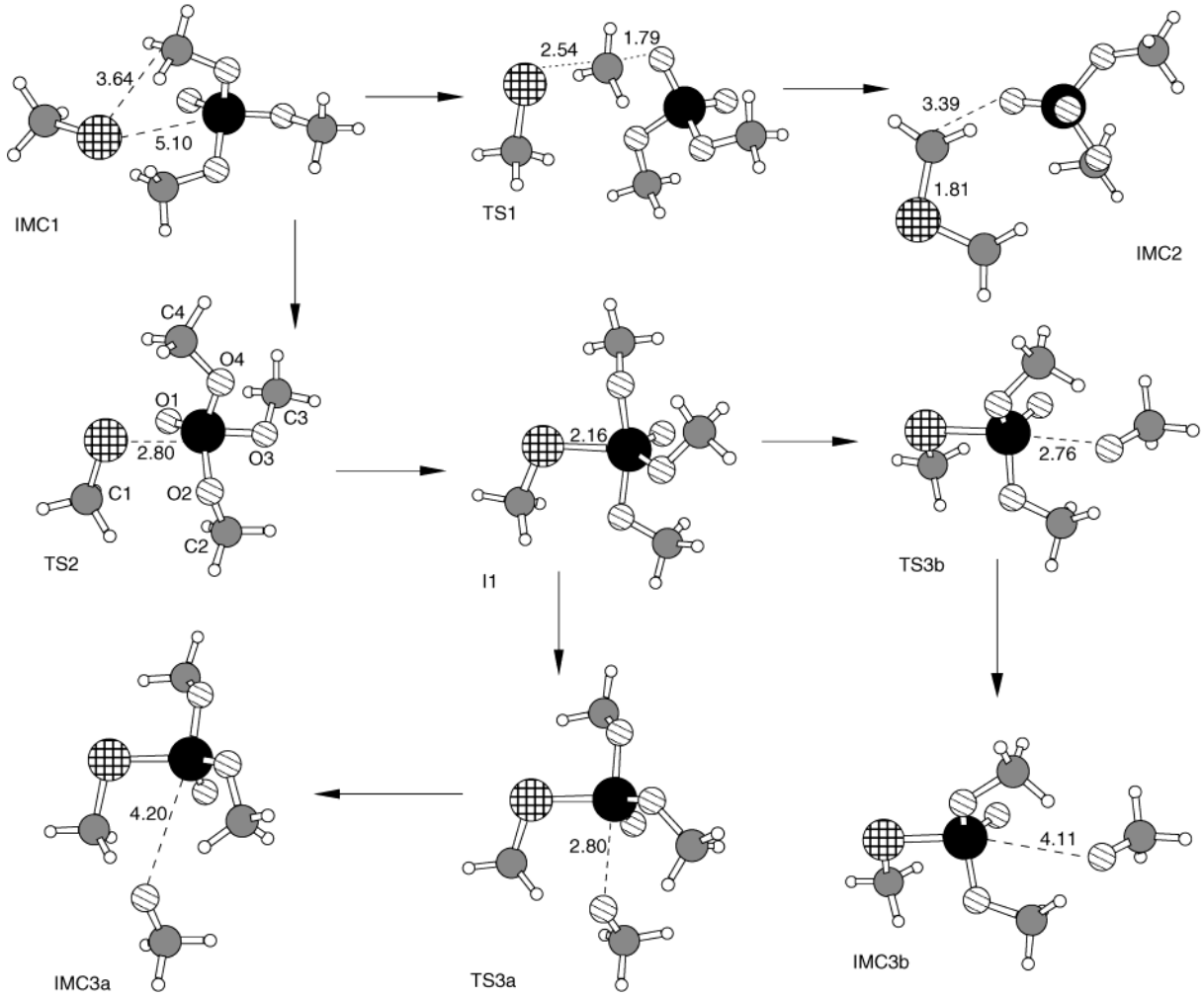

Figure 4. Structures optimized at the MP2/6-311++G* level of ion−molecule complexes, intermediates, and transition states for the gas-phase reactions of $(CH_3S)^-$ with TMP. Calculated atomic distances are shown in Å. Atom type legend: H(white), C(gray), P(black), O(diagonal lines), and S(crosshatch). See TS2 structure for atom numbering.

TABLE 1: Relative Energies, Entropies, and Free Energies for the Thiolysis Reactions[a]

species	ΔE_{MP2} [b]	ΔE_{ZPE} [c]	ΔE_{TRV} [d]	$T\Delta S_{TRV}$ [e]	ΔG(0 K)[f]
Reaction at Carbon					
TMP + $(CH_3S)^-$	0.00	0.00	0.00	0.00	0.00
IMC1	−18.0	0.92	1.80	−3.06	−17.1
TS1	−4.1	−0.36	0.32	−5.33	−4.49
IMC2	−53.3	0.46	1.32	−3.44	−52.9
$(DMP)^-$ + DMET	−41.1	−0.37	−0.77	−2.75	−41.5
Reaction at Phosphorus					
TMP + $(CH_3S)^-$	0.00	0.00	0.00	0.00	0.00
IMC1	−18.0	0.92	1.80	−3.06	−17.1
TS2	−1.96	0.87	0.85	−17.3	−1.09
I1	−7.19	1.25	1.14	−19.9	−5.94
TS3a	13.0	−0.56	−0.49	−16.7	12.4
TS3b	12.4	−0.57	−0.48	−16.7	11.9
IMC3a	9.42	−0.67	−0.08	−10.6	8.75
IMC3b	9.61	−0.73	−0.10	−8.72	8.88
TMDMP + $(CH_3O)^-$	33.5	−2.70	−2.43	0.09	30.8

[a] Relative quantities in kcal/mol. [b] Electronic and nuclear repulsion energy at the MP2/6-311+G* level. [c] Zero-point energy at the MP2/6-31G* level. [d] $E_{trans} + E_{rot} + E_{vib}$, MP2/6-31G* thermal energies at 298 K. [e] $S_{trans} + S_{rot} + S_{vib}$, MP2/6-31G* entropies at 298 K. [f] $G = EMP_2 + E_{ZPE}$, free energy at 0 K.

basis set. Table 1 shows the different energy contributions to the total free energy.

The reaction coordinate was defined as the difference between the breaking and forming bonds. In all figures, zero energy corresponds to the reactants energy at 30 Å separation (trimethyl phosphate in the C_3 conformation and $(CH_3S)^-$ thiolate). A finite separation distance (30 Å) was used in the reactants and products calculations to retain consistence in the total number of vibrational frequencies.

3.1. Attack at Carbon. Figure 1 shows the minimum energy pathway for geometries calculated at the HF and MP2 levels for the $(CH_3S)^-$ attack at TMP carbon. The three TMP carbon atoms are equivalent since the reactant most stable conformer has a C_3 symmetry.[30,31] An initial ion−molecule complex (IMC) of reactants is formed at reaction coordinate −2.17 Å at the MP2 level, IMC1 (Figure 4), which corresponds to the same IMC formed in the TMP phosphorus attack. The complexation free energy for IMC1 is −17.1 kcal/mol (Figure 3, Table 1). The reaction proceeds through the pentacoordinate TS1 at −0.74 Å. The activation free energy is 12.6 kcal/mol (Figure 3). IMC2 is formed at coordinate 1.56 Å and breaks down to (products) dimethyl phosphate monoanion $(DMP)^-$ and dimethyl thioether (Scheme 1). The complexation free energy for IMC2 is 11.4 kcal/mol. The reaction is exoergic (−41.5) kcal/mol and has a one-step S_N2-like mechanism without formation of an intermediate, a A_nD_n reaction, following the IUPAC nomenclature cite.[32] The reverse reaction (IMC2 → IMC1) has a higher barrier, 48.4 kcal/mol.

Inclusion of electron correlation at the MP2 level resulted in more symmetrical calculated geometries than in the HF level.

The only large geometry difference was a 120° torsion in the IMC1 dihedral angle C3−O3−P−O1 (Figure 4), in-line to the forming P−S bond. Conformational differences in isolated TMP were not observed between structures calculated at the MP2 and HF levels.[30] Although stationary points were found at similar reaction coordinates in MP2 and HF levels, the relative energy difference, $\Delta E_{HF} - \Delta E_{MP2}$, which is only −0.8 kcal/mol in IMC1, rises to 4.8 kcal/mol in TS1 and to 9.2 kcal/mol in IMC2.

The TS1 imaginary frequency at the MP2 level is 580 cm^{-1}, indicating a sharp barrier which accounts for the need to freeze both forming and breaking bonds in the geometry optimizations near TS1 (see Methods).

3.2. Attack at Phosphorus. Figure 2 shows the minimum energy pathways for geometries calculated at the HF and MP2 levels for the $(CH_3S)^-$ attack at the TMP phosphorus. After the reactants IMC1 is formed (Figure 4) the reaction proceeds in a stepwise fashion. Initially, the reaction proceeds through (late) TS2 yielding a stable pentavalent trigonal-bipyramidal (TBP) intermediate, I1 (Figure 4). Elimination of methoxide from I1 can proceed through two different pathways, which cross TS3a and TS3b resulting in the products IMC3a and IMC3b, respectively (Figure 4). These complexes can dissociate to the products $(CH_3O)^-$ and thiomethyl dimethyl phosphate (TMDMP, Scheme 1). The thiolysis reaction at phosphorus is endoergic by 30.8 kcal/mol (Figure 3) and has a $A_n + D_n$ [32] mechanism, i.e., a stepwise, associative mechanism with formation of a stable intermediate. The reaction coordinate is defined as the difference between the forming (P−S) and the breaking (P−O) bonds. In the first step, the P−O bond axially positioned to the P−S bond is used.

Three dihedral angle torsions were observed in the reaction leading IMC1 to TS2 (Figure 4). The initial IMC1 has C_s symmetry with the methyl groups of TMP located toward the attacking $(CH_3S)^-$ (Figure 4). The dihedral angle C3−O3−P−O1 rotates from 180° (C_s IMC1) to 60° (C_1) within −2.50 Å in the reaction coordinate (MP2 level). The region between coordinates −1.6 Å and −0.6 Å, calculated at the MP2 level contains TS2 and torsions on dihedrals C1−S−P−O1 and C2−O2−P−O1 which had to be constrained and varied from −25° to 180° and from −65° to 60°, respectively, in addition to the P−S bond length constraint (see Methods). These numerous partial geometry optimizations resulted in an extensive search of the partial MP2 potential energy surface (PES) and possible reaction pathways along the constrained dihedrals and bond length. The minimum energy pathway consisted of C1−S−P−O1 torsion from −25° to 60° at coordinate −1.50 Å and C2−O2−P−O1 torsion from 0° to 57° at coordinate −1.26 Å. No other pathway with similar energetics was found, e.g., constraining C1−S−P−O1 to 60° and varying the reaction coordinate to values smaller than −1.7 Å raised the energy of the calculated structures by 1 kcal/mol for each 0.05 Å variation in the reaction coordinate. The fully optimized distorted TBP TS2 (Figure 4) is found at coordinate −1.16 Å with dihedral angles for C3−O3−P−O1, C1−S−P−O1, and C2−O2−P−O1, of 48°, 64°, and 57°. The O3−P−S angle was 166°, a typical in-line position, while O1, O2, and O4 are equatorial. The TS2 calculated at the HF level was found at coordinate −0.61 Å (0.5 Å closer to I1 than the MP2 structure). The activation free energy for the first step is 16.0 kcal/mol (Figure 3) and the reverse reaction (I1 → IMC1) has a barrier of 4.84 kcal/mol.

The reaction proceeds without other large structural modifications until a practically barrierless pseudorotation at coordinate −0.62 Å moves the in-line O3−P−S, from the axial to an equatorial position. At coordinate −0.48 Å the TBP I1 (see Figure 4) is formed with O1, S, and O3 atoms in equatorial and the other two oxygens (O2 and O4) in axial position. All dihedral angles in I1 are essentially the same as in TS2.

Three different intermediates with different TBP conformations (O1 and O2 axial, S and O2 axial, and O1 and S axial) were analyzed by using MP2 and HF levels. Only I2 (Figure 4), with O1 and O2 axial, and S, O3, and O4 equatorial, was stable in the MP2/6-31G* level. The other two intermediates were unstable in both calculated levels. The relative energy of I2 is plotted in Figure 2 as isolated points at reaction coordinates −0.50 for MP2 and −0.49 for HF level. The I2 intermediate, however, was unstable at the MP2/6-311++G* level. The P−S bond was disrupted, yielding a transition structure.

Two pathways with similar energetics are possible for the second reaction step and both were found at the MP2 and HF levels. The pathway corresponding to TS3b/IMC3b at the HF level is not shown in Figure 2 for the sake of clarity and because it is not significantly different from the TS3a/IMC3a pathway. Following, we describe the MP2 pathway.

The leaving group $(CH_3O)^-$ can be positioned axially to another methoxide as in I1. This pathway leads to another distorted TBP TS3a (Figure 4) at reaction coordinate 0.72 Å and with similar conformations besides torsions of dihedral C3−O3−P−O1 and C1−S−P−O1 angles to −26° and 34°, placing methyl groups closer to the leaving group. The activation free energy for this step is 18.3 kcal/mol. Further displacement of the leaving group forms IMC3a at coordinate 2.03 Å. TS3a is located midway on the reaction pathway with similar distances from I1 (1.2 Å) and IMC3a (1.31 Å).

Another possible pathway involves a barrierless pseudorotation from I1 which replaces the leaving methoxide axially to the $(CH_3S)^-$, similar to the TS2 arrangement, and proceeds to another distorted TBP TS3b (see Figure 4) at coordinate 0.65 Å with dihedrals C3−O3−P−O1 changing to 0° and C4−O4−P−O1 to −25° so that the methyl groups are directed toward the leaving methoxide. This pathway has an activation energy of 17.8 kcal/mol. Finally, IMC3b is formed at coordinate 1.76 Å with a conformation similar to TS3b. TS3b is located midway on the reaction coordinate between I1 (1.13 Å) and IMC3b (1.11 Å).

IMC3a and IMC3b can break down to the same products $(CH_3O)^-$ and TMDMP. The ion−molecule complexation free energy is 22.1 kcal/mol for IMC3a and 22.0 kcal/mol for IMC3b. Note the pathway corresponding to the higher energy TS3a has a lower energy IMC3a. The free energy barriers for the reverse reactions are 3.66 kcal/mol in IMC3a → I1, and 2.98 kcal/mol in the IMC3b → I1.

The partial PES found was smooth and geometries calculated at the MP2 level did not changed significantly from the HF geometries in the two pathways for the second step in the phosphorus reaction. However, large differences were observed between geometries calculated at the MP2 and HF levels for transition states and nonstationary points in the first reaction step. The relative energy differences, $\Delta E_{HF} - \Delta E_{MP2}$, increased substantially from −0.8 kcal/mol in IMC1, to 19.1 kcal/mol in TS2, 21.0 kcal/mol in I1, 18.0 kcal/mol in TS3a, and 13.4 kcal/mol in IMC3a.

The imaginary frequencies at the MP2/6-31G* level contained the forming and breaking bonds motion. Their values are 120 cm^{-1} for TS2, and 114 cm^{-1} for both TS3a and TS3b. The small magnitude of these frequencies indicates a flat surface at the transition state region, in contrast to the sharper barrier in TS1 for the attack at TMP carbon. During the initial vibrational analysis, the IMC1 lowest 6 frequencies were as high as 85

cm^{-1}. The MC1 structure was re-optimized with tighter force and displacement convergence criteria[29] and frequencies were recalculated. The lowest 6 frequencies were smaller than 3 cm^{-1} as all other structures (see Methods).

4. Discussion

The stationary points found at the MP2/6-31G* reaction pathway scan were fully optimized at the MP2/6-311++G* level. The geometries obtained with this larger basis set, including diffuse functions, were very similar to the 6-31G* geometries in general. The larger root mean-squared differences (RMS) between the geometries obtained with the two basis sets were found in the IMC2 (0.87 Å), IMC3b (0.49 Å), and TS3b (0.17 Å). The differences in these three structures are a consequence of relative dihedral angle displacements between the two nonbonded groups (dimethyl thioether and $(DMP)^-$ in IMC2, and TMDMP and $(CH_3O)^-$ in IMC3b and TS3b). The differences in all other structures were smaller than or equal to 0.06 Å. The I2 intermediate was not stable at the MP2/6-311++G* level. The P−S bond was disrupted, yielding the transition state structure, TS2. This was the only qualitative difference found between the two basis sets used here.

The qualitative results and the relative energy profiles were not altered in calculations using the larger basis set (6-311++G*). The differences between the MP2/6-31G* and the MP2/6-311++G* relative energies are smaller than 1.5 kcal/mol in the reaction of $(CH_3S)^-$ at TMP carbon, and in the first step for the reaction of $(CH_3S)^-$ at TMP phosphorus for all the stationary geometries. The relative energy differences are larger in the second step of $(CH_3S)^-$ attack at TMP phosphorus. The MP2/6-311++G* relative energies are 5 and 6 kcal/mol more stable than the MP2/6-31G* energies for the two TS3 and the two IMC3, respectively. The products of reaction at phosphorus, TMDMP and $(CH_3O)^-$ (Scheme 1), are 15 kcal/mol more stable at the MP2/6-311++G*. Although the second step of thiolysis at TMP phosphorus is stabilized, the calculations including diffuse functions and the more complete basis set maintained the general shape of the reaction profiles.

Numerical frequency calculations were carried out for the IMC2 at the MP2/6-311++G* level to probe the influence of the structural changes in the zero-point energy. The difference, $ZPE_{MP2/6-311++G*} - ZPE_{MP2/6-31G*}$, for IMC2 is −1.63 kcal/mol. This value is a reasonable upper bound for the differences between the ZPE calculated for the MP2/6-31G* and MP2/6-311++G* geometries. The deviations in the geometries are consequences of relative dihedral angle displacements between the nonbonded species in the IMCs and in the TSs (see above). Dihedral angles usually have low frequency vibration modes which have a small contribution to the ZPE. We expect that the MP2/6-311++G* structures with RMS differences smaller than 0.06 Å will have relative ZPE very similar to the MP2/6-31G* values. ZPEs are also rather insensitive to the basis set used in frequency calculations.[33] Hence, the MP2/6-31G* ZPE values are suitable for the calculation of the relative free energies (Table 1 and Figure 3).

The free energies of reaction at 0 K for attack at TMP carbon and phosphorus differ by 72.3 kcal/mol (Figure 3). Attack at carbon is very exoergic and thermodynamically favorable. Attack at phosphorus is highly endoergic and unfavorable. This difference is, in most part, due to the much better leaving group ability of the charge-delocalized $(DMP)^-$ than the charge-localized $(CH_3O)^-$ leaving group.[7] The gas-phase acidity of $(DMP)^-$ is between hydrochloric acid and dichloroacetic acid.[7] Attack at carbon is also kinetically more favorable, with an activation barrier smaller, by at least 5 kcal/mol, than those for reaction at phosphorus (Figure 3). The Hammond postulate applies to both the early TS1 and the late TS2. Structurally (Figure 4) and energetically (Figure 3) TS1 is closer to reactants IMC1 and TS2 to intermediate I1. However, the Hammond postulate seems not to apply to TS3a and TS3b which are located half way in the reaction coordinate but are much closer in energy to IMC3a and IMC3b. These thermodynamic and kinetic considerations render not only $(CH_3S)^-$ attack at TMP carbon more feasible and stable in the gas phase but also mean that attack at phosphorus would be reversed since the barriers for return are small (see Results).

Reaction energies and barriers for hydroxide, methoxide, and fluoride nucleophilic attack at TMP (both carbon and phosphorus) were calculated by Lim et al. at the MP2/6-31+G*//HF/6-31+G* level.[11] The reactions at carbon are always exoergic, −56.1 kcal/mol for hydroxide attack and −55.8 kcal/mol for methoxide attack at 0 K. Hydroxide attack at phosphorus results in the same products as attack at carbon because of an internal proton transfer. Methoxide attack at phosphorus is an identity reaction. These calculations by Lim et al. are in agreement with the results presented here and with the general view that $(DMP)^-$ is a better leaving group upon nucleophilic attack at carbon. The actual barrier values are not given in the original paper[11] since only TS energies and not IMC energies are presented. Removing the thermal contribution (see below) and using the author's data we estimated the activation free energies for attack at carbon and phosphorus to be smaller than or equal to 10 kcal/mol at 0 K. Both reactions exhibit A_nD_n mechanisms for attack at carbon and $A_n + D_n$ at phosphorus. There is a pseudorotation in the hydroxide attack at phosphorus which is barrierless as we found in the $(CH_3S)^-$ attack at phosphorus (Figure 2).

Our calculated structures had ca. 1/3 of their normal mode vibrational frequencies below 500 cm^{-1} and most of them were internal rotations and collective angle bendings, not harmonic vibrations. Treatment of these low vibrational modes in the standard harmonic oscillator approximation may lead to substantial errors, especially in S_{vib}.[22] Appropriate calculation of thermodynamic functions from these modes would be lengthy, time-consuming, and would require user intervention. Moreover, only treatment of pure internal rotations are implemented in the program system used here.[25] Collective bending and mixtures with internal rotations require a different approach. One would like to have thermal energies, entropies, and free energies at normal temperature but it is impractical for the reaction system calculated here. It seems more useful to obtain accurate free energy values at 0 K than to obscure the results with inaccurate contributions. We show in Table 1 the values of E_{TRV} and S_{TRV} (translational, rotational, and vibrational contributions to thermal energy and entropy) calculated using standard statistical mechanics[24] during the vibrational analysis.

The transition state geometries found at the HF level may contain inaccuracies because the calculations at this level of theory in reaction coordinates near TS were always steep with high energy changes upon small variations in nuclear configuration for both attack at TMP carbon and phosphorus (for similar discussions see, for example, the book by Shaik, Schelegel, and Wolfe[34]). For this reason we have not further developed on the HF results.

Addition of electronic correlation at the MP2 level resulted in a smooth description of the reaction coordinate near transition state regions. However, the partial PES found in the first step of the attack at TMP phosphorus, between reaction coordinates −1.6 Å and −0.6 Å (see Results, Figure 2), was still irregular.

Variations in the constrained dihedral angles merged such angle changes with the reaction coordinate.

The presence of this rugged and steep topology at the Møller-Plesset (and Hartree-Fock) surface simply shows the lack of sufficient variational flexibility in the electronic wave function calculations. A larger basis-set could extend flexibility in the molecular orbitals. But since the TS regions can be viewed as a crossing between different valence configurations,[34] an increase in the N-electron flexibility, i.e., a multi-determinantal expansion of the electronic wave function, would be necessary to better describe the TS2 region.

Inclusion of electronic correlation is essential for energy calculations and reaction barriers were reduced by more than 18 kcal/mol in the two reaction steps at phosphorus and by 5 kcal/mol in the reaction at carbon from calculations at the HF to the MP2 level.

No direct experimental data are available to compare with our results. Flowing afterglow gas-phase measurements by Lum and Grabowski[7] of the deuterated methoxide, $(CD_3O)^-$, attack on TMP show a rate relation of 43:1 between the reactions at carbon and phosphorus, respectively. This ratio corresponds to a 2.2 kcal/mol difference in the barrier heights in favor of attack at carbon.[35] Using the barriers calculated here for TMP thiolysis, such ratio would be as high as 2×10^7:1, below the detection limit of experimental measurements. Lum and Grabowski also measured the reaction of hydrogen sulfide $(HS)^-$ with TMP and demonstrated a 100% regio-selectivity for attack at carbon. The $(HS)^-$ reaction with TMP carbon[7] is the slower one in a series of nucleophiles which include hydroxide, methoxide, and fluoride. These results, together with the estimated activation barriers,[11] are in qualitative agreement with the calculations presented here which predict a much more favorable reaction of $(CH_3S)^-$ at TMP carbon than at phosphorus and higher barrier for carbon attack than the other nucleophiles.

Several mechanistic issues should also be considered. Pseudorotation is taken to be a common process in the reactions of phosphate esters. Pseudorotation is proposed to involve free energy barriers which may preclude the formation (or reaction) of some intermediates.[7,36,37] Pseudorotation involves the bending of two angles (e.g., TS2 undergoes pseudorotation by changing the angles O3−P−S from 166° to 118° and O4−P−O2 from 118° to 156°, Figure 4) resulting in exchange of equatorial to axial position (and vice versa) of the atoms involved. Here pseudorotations were found in the pathway before and after formation of intermediate, from TS2 to I1 and from I1 to TS3b, and both are essentially barrierless processes (Figure 2). The I1 → I2 pseudorotation would involve a barrier at least as large as the energy difference between the intermediates obtained in the MP2/6-31G* level (Figure 2) and therefore the I2 would not be significantly populated. The I2 intermediate was not stable at the higher MP2/6-311++G* level. In view of the above reasons we have not explored the I1 ⇌ I2 conversion and we consider pseudorotations mechanistically and energetically unimportant for $(CH_3S)^-$ reaction with TMP phosphorus.

Addition of nucleophiles to phosphates forming pentacoordinate TBP intermediate in condensed phase is thought to follow some "preference rules" for the ligand orientation: entering and leaving groups occupy axial, in-line positions, and electronegative groups prefer axial positions.[37] Our results suggest that the entering $(CH_3S)^-$ and leaving $(CH_3O)^-$ groups maintain an axial position of a (distorted) TBP (Figure 4) in the thiolysis at TMP phosphorus. In addition, I1 has the less electronegative thiomethoxide in equatorial and the more electronegative methoxide in axial position. However, one of the two competitive, energetically similar pathways for methoxide elimination from I1 has the leaving $(CH_3O)^-$ axial to the thiomethoxide group. The present calculation indicates that a less electronegative group can occupy an axial position for the leaving group elimination. The in-line displacement is typical of nucleophilic substitution reactions with inversion of configuration, when the entering, leaving, and electrophilic groups are positioned at or near a straight line. This result has not been observed in the other cases of nucleophilic displacement of phosphate esters.[9−11] Our calculations, however, are in agreement with the proposed enzymatic in-line mechanism for phosphorylation of cystein in PTPases.[14]

Lum and Grabowski[7] and Lim et al.[11] also propose that the rate-limiting step in the nucleophilic attack at phosphorus centers is the addition of the entering group and not pseudorotations or the elimination of the leaving group. Lum and Grabowski also note that if elimination were to be rate-limiting, some product from addition at phosphorus and scramble of the TBP intermediate would be experimentally observed. That is not the case in the TMP phosphorus thiolysis where the rate-limiting step is the elimination of $(CH_3O)^-$ (Figure 3) from I1. Products from $(CH_3S)^-$ (or $(HS)^-$ in the experimental work) attack at phosphorus are difficult to detect on account of the large elimination barrier, the small decomposition barrier in the reverse reaction, and the large overall unfavorable thermodynamics of reaction (see above and Figure 3).

The age-old question of whether phosphate esters react by associative or dissociative mechanisms[18] on attack at phosphorus depends on the alkylation and charge of the ester. Monoalkyl (mono- or di-) anionic phosphate esters are generally believed to react by dissociative, $D_n + A_n$, mechanisms.[18] Recent calculations by Warshel et al.[9,38,39] have raised the possibility of associative mechanisms for hydrolysis and alcoholysis of monoalkyl phosphates. Trimethyl phosphates are considered to react through TBP intermediates and $A_n + D_n$ mechanisms.[18] Lim et al. found these mechanisms for three different nucleophiles reacting toward TMP (Warshel et al.[39] computes only the first step of TMP hydrolysis). The results presented here agree with this general trend. It remains to be seen which are the mechanisms for the reaction of thiol nucleophiles with mono- and dialkyl phosphate esters. PTPases catalyze the hydrolysis of monoalkyl phosphate anions by a transient formation of a thiophosphate with the cystein side-chain.[14] PTPases should therefore be able not only to stabilize the large electrostatic repulsion found in this configuration but also to overcome the large activation energy barrier found here for $(CH_3S)^-$ attack at phosphorus if the same mechanism found in the triester thiolysis in the gas phase is followed in the enzyme active site.

In aqueous phase the free energy profile for this reaction can be significantly altered. The charge localized species, i.e., minima IMC1, I1, IMC3a, and IMC3b, should have larger solvation energies (in module) than the charge delocalized species, TS1, TS2, TS3a, TS3b, and IMC2. This can result in larger stabilization of the products of attack in TMP phosphorus than the carbon attack products and in larger activation barriers for both reactions. The more polarizable $(CH_3S)^-$ should have solvation energy smaller (in module) than $(CH_3O)^-$ what could result in a less endoergic thiolysis of TMP phosphorus in solution.

5. Conclusions

We have presented ab initio calculations on the thiolysis reaction of trimethyl phosphate (TMP) in the gas phase. Attack at carbon is thermodynamically and kinetically more favorable

than attack at phosphorus. Reaction at carbon is exoergic and is a typical A_nD_n, pentacoordinate substitution. Reaction at phosphorus is endoergic and has a $A_n + D_n$ mechanism with formation of a stable TBP intermediate. The transition state surface around TS2 is very rugged where similar nuclear configurations have rather different energy. Future work includes multi-configurational (e.g., MCSCF) electronic structure calculations of this reaction region. Two different but equally probable pathways are possible for the elimination of methoxide from I1, one contains a novel arrangement with the less electronegative $(CH_3S)^-$ in-line with the leaving group. We are now investigating the enzymatic mechanisms which render PTPases as effective catalysts for thiolate attack at phosphorus centers in phosphate esters.

Acknowledgment. We acknowledge a fellowship (G.M.) and financial support from FAPESP (Fundação de Amparo a Pesquisa do Estado de São Paulo), the computational resources of LCCA (Laboratório de Computação Científica Avançada − Universidade de São Paulo), and Dr. Luis Gustavo Dias for helpful discussions.

References and Notes

(1) Westheimer, F. H. *Science* **1987**, *235*, 1173.
(2) Cox, J. R.; Ramsay, O. B. *Chem. Rev.* **1964**, *64*, 317.
(3) Bunton, C. A. *Acc. Chem. Res.* **1970**, *3*, 257.
(4) Bunton, C. A.; Gillit, N. D.; Kumar, A. *J. Phys. Org. Chem.* **1997**, *10*, 221.
(5) Thatcher, G. R. J.; Kluger, R. *Adv. Phys. Org. Chem.* **1989**, *25*, 99.
(6) Hodges, R. V.; Sullivan, S. A.; Beauchamp, J. L. *J. Am. Chem. Soc.* **1980**, *102*, 935.
(7) Lum, R. C.; Grabowski, J. J. *J. Am. Chem. Soc.* **1992**, *114*, 8619.
(8) Asubiojo, O. I.; Brauman, J. I.; Levin, R. H. *J. Am. Chem. Soc.* **1977**, *99*, 7707.
(9) Florian, J.; Warshel, A. *J. Phys. Chem. B* **1998**, *102*, 719.
(10) Dejaegere, A.; Liang, X.; Karplus, M. *J. Chem. Soc., Faraday Trans.* **1994**, *90*, 1763.
(11) Chang, N.; Lim, C. *J. Phys. Chem. A* **1997**, *101*, 8706.
(12) Dantzman, C. L.; Kiessling, L. L. *J. Am. Chem. Soc.* **1996**, *118*, 11715.
(13) Ahn, N.; Ed. Special Issue: Protein Phosphorylation and Signaling; *Chem. Rev.* **2001**, *101*.
(14) Jackson, M. D.; Denu, J. M. *Chem. Rev.* **2001**, *101*, 2313.
(15) Barford, D.; Das, A. K.; Egloff, M. P. *Annu. Rev. Biophys. Biomol. Struct.* **1998**, *27*, 133.
(16) Zhang, Z. Y.; Dixon, J. E. *Biochemistry* **1993**, *32*, 9340.
(17) Pannifer, A. D. B.; Flint, A. J.; Tonks, N. K.; Barford, D. *J. Biol. Chem.* **1998**, *273*, 10454.
(18) Cleland, W. W.; Hengge, A. C. *FASEB J.* **1995**, *9*, 1585.
(19) Admiraal, S.; Herschlag, D. *J. Am. Chem. Soc.* **2000**, *122*, 2145.
(20) Yliniemeia, A.; Uchimaru, T.; Tanabe, K.; Taira, K. *J. Am. Chem. Soc.* **1993**, *115*, 3032.
(21) Lim, C.; Karplus, M. *J. Am. Chem. Soc.* **1990**, *112*, 5872.
(22) Ayala, P.; Schlegel, H. B. *J. Chem. Phys.* **1998**, *108*, 2314.
(23) Mercero, J. M.; Barrett, P.; Lam, C. W.; Fowler, J. E.; Ugalde, J. M.; Pedersen, L. G. *J. Comput. Chem.* **2000**, *21*, 43.
(24) McQuarrie, D. A. *Statistical Thermodynamics*; Harper and Row: New York, 1973.
(25) Frisch, M. J., et al. *Gaussian 98, Rev. A.9*; Gaussian Inc.: Pittsburgh, PA, 1998.
(26) Møller, C.; Plesset, M. S. *Phys. Rev.* **1934**, *46*, 618.
(27) Fukui, K. *Acc. Chem. Res.* **1981**, *14*, 363.
(28) Gonzalez, C.; Schlegel, H. B. *J. Phys. Chem.* **1990**, *94*, 5523.
(29) Ochterski, J. W. *White Paper: Vibrational Analysis in Gaussian*; Guassian Inc.: Pittsburgh, PA, 1999. http://www.Gaussian.com.
(30) George, L.; Viswanathan, K. S.; Singh, S. *J. Phys. Chem. A* **1997**, *101*, 2459.
(31) Streck, R.; Barnes, A. J.; Herrebout, W. A.; vanderVeken, B. J. *J. Mol. Struct.* **1996**, *376*, 277.
(32) Guthrie, R. D.; Jencks, W. P. *Acc. Chem. Res.* **1989**, *22*, 343.
(33) Pople, J.; Scott, A.; Wong, M.; Radom, L. *Isr. J. Chem.* **1993**, *33*, 345.
(34) Shaik, S. S.; Schlegel, H. B.; Wolfe, S. *Theoretical Aspects of Physical Organic Chemistry: The SN2 Mechanism*; Wiley: New York, 1992.
(35) Billing, G. D.; Mikkelsen, V. *Introduction to molecular dynamics and Chemical kinetics*; John Wiley: New York, 1996.
(36) Chang, N. Y.; Lim, C. *J. Am. Chem. Soc.* **1998**, *120*, 2156.
(37) Westheimer, F. H. *Acc. Chem. Res.* **1968**, *1*, 70.
(38) Florian, J.; Åqvist, J.; Warshel, A. *J. Am. Chem. Soc.* **1998**, *120*, 11524.
(39) Florian, J.; Warshel, A. *J. Am. Chem. Soc.* **1997**, *119*, 5473.